HHS Public Access

Author manuscript

Arch Toxicol. Author manuscript; available in PMC 2015 August 01.

Published in final edited form as:

Arch Toxicol. 2015 July ; 89(7): 1057–1070. doi:10.1007/s00204-014-1302-y.

Tetramethylpyrazine (TMP) protects against sodium arsenite-induced nephrotoxicity by suppressing ROS production, mitochondrial dysfunction, pro-inflammatory signaling pathways and programed cell death

Xuezhong Gong,
Center for Radiological Research, Columbia University, 630 West 168th Street, New York, NY 10032, USA

Department of Nephrology, Shanghai Municipal Hospital of Traditional Chinese Medicine, Shanghai University of Traditional Chinese Medicine, 274 Zhijiang Middle Road, Shanghai 200071, China

Vladimir N. Ivanov,
Center for Radiological Research, Columbia University, 630 West 168th Street, New York, NY 10032, USA

Mercy M. Davidson, and
Department of Radiation Oncology, College of Physician and Surgeons, Columbia University, 630 West 168th Street, New York, NY 10032, USA

Tom K. Hei
Center for Radiological Research, Columbia University, 630 West 168th Street, New York, NY 10032, USA

Department of Radiation Oncology, College of Physician and Surgeons, Columbia University, 630 West 168th Street, New York, NY 10032, USA

Xuezhong Gong: shnanshan@hotmail.com

Abstract

Although kidney is a target organ of arsenic cytotoxicity, the underlying mechanisms of arsenic-induced nephrotoxicity remain poorly understood. As tetramethylpyrazine (TMP) has recently been found to be a renal protectant in multiple kidney injuries, we hypothesize that TMP could suppress arsenic nephrotoxicity. In this study, human renal proximal tubular epithelial cell line HK-2 was used to elucidate the precise mechanisms of arsenic nephrotoxicity as well as the protective mechanism of TMP in these cells. Sodium arsenite exposure dramatically increased cellular reactive oxygen species (ROS) production, decreased levels of cellular glutathione (GSH), decreased cytochrome *c* oxidase activity and mitochondrial membrane potential, which indicated mitochondrial dysfunction. On the other hand, sodium arsenite activated pro-inflammatory signals,

Correspondence to: Xuezhong Gong, shnanshan@hotmail.com.

Conflict of interest The authors declare that they have no conflict of interest.

including β-catenin, nuclear factor-κB (NF-κB), p38 mitogen-activated protein kinase (MAPK), tumor necrosis factor alpha and cyclooxygenase-2 (COX-2). Small molecule inhibitors of NF-κB and p38 MAPK blocked arsenic-induced COX-2 expression, suggesting arsenic-induced COX-2 upregulation was NF-κB- and p38 MAPK-dependent. Finally, sodium arsenite induced autophagy in HK-2 cells at early phase (6 h) and the subsequent apoptosis at 24 h. Treatment by TMP or by the antioxidant *N*-acetylcysteine decreased arsenic-induced ROS production, enhanced GSH levels, prevented mitochondria dysfunction and suppressed the activation of pro-inflammatory signals and the development of autophagy and apoptosis. Our results suggested that TMP may be used as a new potential therapeutic agent to prevent arsenic-induced nephrotoxicity by suppressing these pathological processes.

Keywords

Sodium arsenite; Tetramethylpyrazine (TMP); Nephrotoxicity; Mitochondrial dysfunction; Cyclooxygenase-2; Autophagy

Introduction

Arsenic is a major environmental contaminant of global scale and arsenic exposure could result in cancer of the skin, liver, bladder, kidney and lung, as well as, cardiovascular disease, developmental and reproductive abnormalities (Michael 2013; Rodriguez-Lado et al. 2013; Yu et al. 2013). In spite of its adverse health effects, short-term, acute arsenic exposure has clinical, therapeutic values in the treatment of acute promyelocytic leukemia (APL) and other solid tumors (Yu et al. 2013). As one of the main arsenic excretion pathways in the human body, kidney is a target organ of arsenic cytotoxicity. Therefore, arsenic exposure either from environmental contamination or as a result of clinical application may lead to kidney damage, including renal failure, proteinuria and increased urinary excretion of protein biomarkers for acute kidney injury (AKI) (Chen et al. 2011; Soignet et al. 1998; Yu et al. 2013; Emadi and Gore 2010). For APL patients with impaired renal function, only about 40 % of the excessive plasma arsenic from chemotherapeutic regimen could be removed by hemodialysis (Yamamoto et al. 2009). Based on recent epidemiologic studies in a rural US population, and in some regions of China, Taiwan and, especially, in Bangladesh, arsenic is a major risk factor for kidney disease and arsenic nephrotoxicity should, therefore, receive significantly more attention (Chen et al. 2011; Zheng et al. 2013).

The mechanism(s) contributing to arsenic nephrotoxicity are poorly understood. Reactive oxygen species (ROS), which are generated during metabolic activation of the metalloid, and the ensuring oxidative stress are hypothesized to be critical initiating events in arsenic nephrotoxicity (Yen et al. 2012). In both AKI and chronic kidney disease (CKD), oxidative stress and inflammation, which are tightly linked, are characteristic features (Ruiz et al. 2013). Cyclooxygenase-2 (COX-2), a pro-inflammatory, inducible enzyme, has recently been shown to be up-regulated after arsenic exposure in human lung fibroblasts (Wang et al. 2013b) and human uroepithelial cells (Wang et al. 2013a). It is well documented that COX-2 plays a key role in kidney development and COX-2-derived prostanoids are essential in

maintaining renal function (Hao and Breyer 2007). However, to our knowledge, the role of COX-2 in arsenic nephrotoxicity has not been previously studied. As a redox-sensitive transcription factor, nuclear factor (NF)-κB regulates COX-2 gene expression in concert with other pro-inflammatory and anti-inflammatory factors (Ruiz et al. 2013).

Previous work from our laboratory has clearly shown that mitochondria are an important target of the mutagenic and metabolic effects of arsenic in mammalian cells (Partridge et al. 2007). Recently, arsenic has also been reported to induce autophagy (Lau et al. 2013), which is an important mechanism regulating cell survival and death in connection with mitochondrial functions (Graef and Nunnari 2011). We therefore want to further elucidate the respective roles and relationship between ROS production, autophagy, mitochondrial dysfunction and inflammation in arsenic-induced nephrotoxicity, which is not well understood so far.

2,3,5,6-Tetramethylpyrazine (TMP) is a compound extracted from the Chinese medicinal plant Ligusticum wallichi (Chuanxiong) (Zhai et al. 2012; Wu et al. 2011). In addition to vasodilatory and antiplatelet activities, TMP also functions as an antioxidant, an anti-inflammatory agent and a suppressor of apoptosis (Tang et al. 2013; Zhai et al. 2012; Gong et al. 2013). TMP has been reported to prevent kidney injury induced by the contrast medium iohexol, gentamycin, diabetes and cisplatin (Juan et al. 2007; Gong et al. 2013). Thus, we hypothesized that TMP may suppress arsenic nephrotoxicity. To address this problem, we have further investigated in the present study the regulatory effects of TMP on the pro-inflammatory signaling pathways induced by arsenic treatment and possible mechanisms involved in TMP-mediated protection against arsenic-induced nephrotoxicity.

Materials and methods

Materials

All chemicals were purchased from Sigma Chemicals (St. Louis, Mo., USA) unless otherwise stated. NF-κB inhibitor Bay11-7082 was obtained from Calbiochem (La Jolla, CA, USA).

Cell culture and treatment

The human proximal tubular cell line (human kidney 2 or HK-2) was obtained from the American Type Culture Collection (Manassas, VA, USA) and grown in serum-free keratinocyte-cultured medium supplemented with epidermal growth factor (5 ng/ml) and bovine extract (50 μg/ml), penicillin and streptomycin at 37 °C in a 5 % CO_2 humidified environment. About 50 mM stock sodium arsenite was used at the final concentrations of 1–10 μM. *N*-Acetylcysteine (NAC 10 mM), TMP (50 μM, 100 μM), Bay (5 μM) and SB 203580 (SB, inhibitor of p38 MAPK, 10 μM) were used either alone or in combination with arsenic and were added into media 30 min before arsenic treatment.

Cell viability analysis

3-(4,5-Dimethylthiazol-2-yl)-2,5-diphenyltetrazolium (MTT) assay was used to determine cell viability. Briefly, cells were seeded on 96-well plates at a density of 5,000 cells/well and

cultured at 37 °C for 24 h, before exposed to arsenic at concentrations ranging from 1 to 200 μM for 6, 24 and 48 h. After treatment, the supernatant was removed and 100 μl MTT solution (0.5 mg/ml in DMEM) was added for a further 3-h incubation at 37 °C. Subsequently, crystals were dissolved in DMSO. The extent of the reduction of MTT was quantified by measuring absorbance at 550 nm.

TUNEL staining

To determine levels of apoptotic cell death, terminal deoxynucleotidyl transferase-mediated dUTP-biotin nick-end labeling (TUNEL) staining was performed using a Click-iT TUNEL Alexa Fluor 488 Imaging Assay (Invitrogen, Grand Island, NY, USA) according to the manufacturer's instructions with the exception that propidium iodide (PI) replaced Hoechst 33342 to label all nuclei. Stained nuclei were analyzed by a Nikon confocal microscope (Nikon TE200-C1) at 24 °C room temperature. TUNEL-positive cell numbers from 20 different fields (a total of 2,000–2,500 cells) were counted to get an average number of apoptotic cells per field.

Determination of apoptosis levels and cell cycle analysis by fluorescence-activated cell sorter (FACS) assay

After treatment, HK-2 cells were permeabilized in 70 % ethanol at 4 °C for at least 24 h. After 30-min staining with PI in the dark at 37 °C (Gong et al. 2010), apoptotic level and cell cycle distribution were evaluated by FACS (a total of 20,000 events were counted). Data were analyzed using CellQuest program. Apoptotic levels were calculated by evaluating the percentage of cells accumulated in the sub-G1 position. Samples were analyzed in triplicates, and independent experiments were repeated 3 times.

Autophagy detection by immunocytochemical staining of LC3B

Autophagy was visualized using LC3B Antibody Kit for Autophagy (Invitrogen) according to the manufacturer's instructions. Briefly, cells were grown on glass cover in 6-well plate and treated with sodium arsenite for 6 h and fixed with 3.7 % formaldehyde in PBS and permeabilized with 0.2 % Triton X-100 in PBS. Rabbit anti-LC3B primary antibody was diluted in blocking buffer (1:500) and incubated 1 h at room temperature. After washing three times with PBS, cells were incubated with anti-rabbit secondary antibody followed by mounting with PI. Image was captured using a Nikon confocal microscope (Nikon TE200-C1) at 24 °C room temperature. Number of autophagosome positive cell was counted. In addition, LC3B protein expression was measured with Western blotting.

Intracellular ROS and glutathione detection

Dihydroethidium (DHE, Invitrogen, Eugene, OR) was used to detect intracellular superoxide production. After 24 h of sodium arsenite treatment, cells were exposed to 2 μM DHE for 45 min at 37 °C in the dark. Subsequently, cells were washed twice with PBS, and FACS analysis was performed using CellQuest program (Becton–Dickinson, Franklin Lakes, NJ, USA). Samples were analyzed in triplicates, and all experiments were independently repeated 3 times.

Glutathione (GSH) levels were determined using Glutathione Assay Kit (Sigma, MO, USA) according to the manufacturer's instructions. The yellow product, 5-thio-2-nitrobenzoic acid (TNB) was measured spectrophoto-metrically at 412 nm. The assay used a standard curve of reduced GSH to determine the amount of GSH in the samples. Samples were analyzed in triplicates, and all experiments were independently repeated 3 times.

Mitochondrial function assay: cytochrome *c* oxidase (Cox) and succinate dehydrogenase (SDH) histochemistry

Histochemical staining for Cox and SDH was performed using previously published method (Salviati et al. 2002). Briefly, cells were cultured on glass cover slips inside 6-well plate. After 6 h of indicated treatment, cells on glass cover were allowed to dry at room temperature for 1 h. Following a 15-min preincubation at room temperature with 1 mM $CoCl_2$ and 50 μl DMSO in 50 mM Tris–HCl, pH 7.6, containing 10 % sucrose, all samples were rinsed once in PBS and incubated for another 3 h with the substrate (10 mg cytochrome *c*, 10 mg of DAB Hydrochloride, 2 mg of catalase and 25 μl DMSO dissolved in 10 ml 0.1 M sodium phosphate, pH 7.6). After rinsing three times with PBS, all samples were mounted on warm glycerin-gelatin and observed under Nikon LABOPHOT-2 microscope to capture images with SPOT Basic TM software. Quantification of histochemical staining was performed with Image J software (NIH) and evaluated by two independent and blinded investigators. Camera light settings were standardized, and color images were captured with 40× objective.

Mitochondrial membrane potential

Mitochondrial membrane potential was measured using Rhodamine 123 staining (Invitrogen) according to the manufacturer's instructions. Briefly, cells were grown on 6-well plate and treated with sodium arsenite for 6 h and then stained with Rhodamine 123 (10 μM final concentration in medium) at 37 °C for 30 min. Image was captured with a Nikon confocal microscope (Nikon TE200-C1) at 24 °C room temperature. Relative fluorescence intensity was quantified by Image J software (NIH).

Western blotting

After the various treatments, whole cell lysates were prepared using RIPA buffer (Invitrogen) containing protease inhibitors. Nuclear extracts were prepared using methods described previously (Schreiber et al. 1989). Protein concentrations were determined with Bio-Rad DC protein assay (Bio-Rad Laboratories, CA, USA) using bovine serum albumin as a standard. After SDS-PAGE, protein samples were transferred to PVDF membrane. Primary antibodies used included: rabbit anti-LC3B, rabbit anti-PARP1, rabbit anti-pro caspase-9, rabbit anti-NF-κB, rabbit anti-TNF-α, rabbit anti-β-catenin, rabbit anti-p38 MAPK, rabbit anti-phospho-p38 MAPK, rabbit anti-histone H3 (Histone) (cell signaling), rabbit anti-COX-2 (Cayman Chemical) and mouse monoclonal anti-β-actin (sigma).

Statistical analysis

All data were presented as mean ± SD for a minimum of three independent experiments in triplicate. All comparisons were made using either one-way ANOVA or a two tailed *t* test

analysis depending on how many conditions were compared in each experiment. One-way ANOVA was followed by Tukey's post hoc test. A value of $p < 0.05$ was considered significant.

Results

Arsenic-induced dose- and time-dependent cell death in HK-2 cells

In our initial experiments on arsenic cytotoxicity in HK-2 cells, trivalent arsenite (sodium arsenite) and pentavalent arsenate (sodium arsenate) were used. Based on determination of cell viability using MTT assay (Fig. 1a, b), both sodium arsenite and sodium arsenate showed a dose- and time-dependent cytotoxicity in HK-2 cells. With the same dose, trivalent arsenite was found to be more cytotoxic than pentavalent arsenate. Indeed, a 10-μM sodium arsenite reduced cell viability to 80.6 and 44.5 % at 24 h and 48 h, respectively (Fig. 1a). In contrast, a similar dose of sodium arsenate resulted in greater than 80 % survival at both time points examined. As shown in Fig. 1a, sodium arsenite toxicity increased sharply if concentration exceeds 10 μM. Given the fact that a dose range of 2.0–10-μM arsenic is clinically relevant in the treatment of APL (Ivanov and Hei 2004, 2005; Shen et al. 1997), we therefore choose this dose range for our study.

TMP and NAC attenuated arsenic-induced cytotoxicity and apoptosis

As shown in Fig. 1a, clinically relevant dosage of sodium arsenite caused significant death of HK-2 cells at 48 h; therefore, we choose 48 h as the time point to determine the protective effects of NAC and TMP against arsenite-induced cytotoxicity. Figure 2a demonstrated that 10 mM NAC and 100 μM TMP pretreatment significantly protected cells from sodium arsenite (10 μM)-induced cytotoxicity. Furthermore, HK-2 cells were cultured in the presence of 10 mM NAC or 100 μM TMP for 48 h, then MTT assay was performed to investigate a potential cytotoxicity of 10 mM NAC or 100 μM TMP. The results indicated that 10 mM NAC and 100 μM TMP were not harmful to HK-2 cells (data not shown).

In the present study, several approaches were used to evaluate arsenic-induced apoptosis in HK-2 cells, such as TUNEL staining, cell cycle-apoptosis assay and detection of caspase activation followed by PARP cleavage that are recognizable markers for apoptosis. A 3.2-fold increase in TUNEL-positive cell number was observed 24 h after 10 μM sodium arsenite treatment (Fig. 1c, d). To further assess whether sodium arsenite treatment affected cell cycle and induced apoptosis, HK-2 cells were stained with PI and analyzed by FACS assay. As shown in Fig. 2, exposure to sodium arsenite (2.5–10 μM) significantly changed cell cycle distribution and induced apoptosis in a dose-dependent manner (Fig. 2a). Additionally, a significant down-regulation of pro caspase-9 (that reflected its activation) and caspase-3-dependent cleavage of PARP1 were revealed by Western blotting 24 h after exposure to sodium arsenite (Fig. 2c). Pretreatment with 100 μM TMP or 10 mM NAC efficiently prevented arsenic-induced apoptosis in HK-2 cells that was evidenced by the significant decrease in TUNEL-positive cell number (Fig. 1c, d) and decreased percentage of cells in the apoptotic sub-G1 area (Fig. 2a, b).

Arsenic-induced autophagy in the early phase of exposure

We first confirmed the occurrence of autophagy during arsenic exposure in human proximal tubular cells. As shown by Western blotting analysis in Fig. 3a, the protein expression of autophagy marker LC3B was markedly increased after 6-h arsenic exposure using three different concentrations, compared with control cells. Interestingly, such an up-regulation was only detected in the early phase, while LC3B protein level was reduced to normal or lower 24 h after arsenic exposure (Fig. 3b). Both NAC and TMP pretreatment could reverse such an increase in LC3B expression levels at 6 h (Fig. 3a, b).

In addition, autophagolysosome formation was detected using anti-LC3B staining and confocal fluorescence microscopy. Indeed, arsenic exposure (2.5–10 μM) notably up-regulated LC3B-positive cell number (about 40 % increase after 6 h of treatment) (Fig. 3c, d). Similarly to the results obtained with analysis of apoptosis, 10 mM NAC and 100 μM TMP significantly decreased a number of LC3B-positive cells (Fig. 3c, d).

TMP and NAC suppressed arsenic-induced intracellular ROS production and enhanced GSH levels

After 24 h treatment with sodium arsenite, the intracellular ROS production was elevated in a dose-dependent manner (Fig. 4a, b). Quantification of the mean fluorescence intensity of images showed that 2.5, 5 and 10 μM sodium arsenite at 24 h increased intracellular ROS levels by 1.6-fold, 2.0-fold and 2.4-fold, respectively, over control levels. Furthermore, 3-h exposure to 10 μM sodium arsenite led to detectable increase in intracellular ROS production in HK-2 cells (Fig. 4c, d). In the presence of NAC (10 mM) or TMP (100 μM), the intracellular superoxide production induced by 3 h (Fig. 4c, d) or 24 h (Fig. 4e, f) arsenic exposure was significantly reduced ($p < 0.05$).

As shown in Fig. 4g, the intracellular GSH level was diminished about 2-fold after 24-h sodium arsenite treatment in HK-2 cells ($p < 0.01$ vs. control). However, both 10 mM NAC and 100 μM TMP pretreatments significantly prevented sodium arsenite-induced GSH down-regulation ($p < 0.05$).

TMP and NAC reversed the decreased mitochondrial membrane potential induced by sodium arsenite exposure

Using Rhodamine 123 staining, we analyzed changes in mitochondrial membrane potential after sodium arsenite treatment of HK-2 cells with or without antioxidant co-treatment. As shown in Fig. 5a, b, arsenic treatment reduced the mitochondrial membrane potential almost twofold; the relative fluorescence intensity of control cells was 30.2 %, while the 10-μM arsenic treatment reduced this level to 14.3 %. Interestingly, NAC and TMP showed significant protection of mitochondrial membrane potential in arsenite-treated cells resulting in mean fluorescence levels of 28.6 and 27.4 %, respectively.

Arsenite-induced mitochondrial dysfunction measured by cytochrome *c* oxidase (Cox) and succinate dehydrogenase (SDH) histochemistry

Cytochrome *c* oxidase (Cox), a subunit of Complex IV of the respiratory chain, is composed of both nuclear and mitochondrially encoded subunits. Changes in Cox levels indicate the

status of mitochondrial respiratory chain function. As shown in Fig. 5c, d, sodium arsenite treatment induced a more than fivefold decrease in Cox enzyme activity in HK-2 cells that was indicative of mitochondrial dysfunction. Compared with Cox, the enzyme activity of succinate dehydrogenase (SDH), or complex II, which is encoded entirely by nuclear DNA, was not significantly impaired by arsenite treatment (Fig. 5e, f). Both NAC (10 mM) and TMP (100 μM) prevented a decrease in Cox activity while showed minimal effect on SDH (Fig. 5c, f).

Sodium arsenite activated pro-inflammatory signaling response, including NF-κB, β-catenin, p38 MAPK and their targets COX-2 and TNF-α in HK-2 cells

The critical role of transcription factor NF-κB in regulation of inflammatory response and carcinogenesis, as well as in modulating environmental toxicant induced pathogenesis has been well established (Baeuerle and Henkel 1994). However, arsenic exposure demonstrated distinct, cell-specific effects on transcription factor NF-κB activation (Kumagai and Sumi 2007). In order to explore the precise role of arsenite in the activation of NF-κB in HK-2 cells, we monitored phospho-NF-κB (Ser536) nuclear protein levels after arsenite treatment. As shown in Fig. 6a, b, the nuclear NF-κB protein levels were up-regulated in a dose-dependent manner, as early as 3 h after arsenite exposure, further increased at 6 h and partially decreased 24 h after treatment. Furthermore, both antioxidant NAC and TMP efficiently decreased arsenite-induced nuclear NF-κB activation in HK-2 cells (Fig. 6a, b) highlighting a role of ROS in NF-κB activation. Similarly, β-catenin protein expression was up-regulated 3 and 6 h after arsenite treatment, but then gradually dropped (Fig. 6c, d). Meanwhile, arsenite-treated HK-2 cells showed an increase in p38 MAPK activities 6 h after treatment (Fig. 7a, b). TMP and NAC showed similar effects on suppressing β-catenin and p38 MAPK activation (Figs. 6a, d, 7a, b).

Furthermore, expression of COX-2, a critical proinflammatory protein, was significantly increased at 3 h, peaked at 6 h and then dropped to basal level at 24 h after sodium arsenite exposure (Fig. 7c, d). TMP and NAC prevented the arsenic-induced COX-2 protein expression (Fig. 7c, d). Interestingly, Bay11-7082 (5 μM, a specific inhibitor of NF-κB activation) and SB203580 (10 μM, an inhibitor of p38 MAPK) blocked arsenic-induced up-regulation of COX-2 expression at 6 h (Fig. 8a, b), indicating that arsenite-induced COX-2 up-regulation was NF-κB and p38 MAPK-dependent.

We also tested protein expression of another crucial proinflammatory factor TNF-α 6 h after sodium arsenite exposure. As shown in Fig. 8c, d, TNF-α protein levels were obviously up-regulated after 6 h arsenite exposure, while TMP and NAC efficiently suppressed such up-regulation of TNF-α, highlighting a strong anti-inflammatory functions of both antioxidants.

Discussion

In the present study, using a human proximal tubular cell line, we examined arsenic-induced nephrotoxicity and the corresponding mechanisms. We demonstrated a dose-dependent cytotoxicity of arsenic in the HK-2 cell model within a clinically relevant dose range of 2–10 μM (Ivanov and Hei 2005; Zhao et al. 2008). Our results provide supporting evidence that arsenite used in the clinic for cancer treatment might increase the risk for kidney

damage. Additionally, our results further suggest that arsenic-induced nephrotoxicity is associated with intracellular ROS production, mitochondrial dysfunction, activations of COX-2 as well as other pro-inflammatory signals and, finally, with programed cell death. All these effects of arsenic could be suppressed by TMP, a potent antioxidant and anti-inflammatory agent extracted from the Chinese Herb, *Ligusticum wallichi*, and by the antioxidant NAC, implying that ROS and inflammation played critical roles for mediating arsenic nephrotoxicity. Interestingly, TMP was used at substantially lower doses (50–100 μM), compared with NAC (10 mM).

Initial experiments were conducted to test the cytotoxicity of sodium arsenite and sodium arsenate in HK-2 cells. Consistent with previous reports (Peraza et al. 2003; Ivanov and Hei 2013; Fan et al. 2010; Martin-Pardillos et al. 2013), we found that the trivalent arsenite showed higher toxicity than the pentavalent arsenate. For sodium arsenite, the 10-μM concentration acted as a threshold dose for treatment period up to 24 h with increased toxicity following either higher dose or longer treatment time (Fig. 1). This finding was consistent with previously studies (Peraza et al. 2003; Ivanov et al. 2013). Acute exposure to arsenic and other common toxic metals are generally characterized by renal tubular necrosis (Eichler et al. 2006). In the present study, we demonstrated programed cell death (via apoptosis and autophagy) was also critically involved in arsenic-induced nephrotoxicity. Recently, arsenic-induced autophagy was observed in human lymphoblastoid cells and HEK293 cell line (Bolt et al. 2010; Lau et al. 2013). According to our results, autophagy occurred in the early phase after arsenic exposure (6 h), which was confirmed by increase in the autophagy marker, LC3B protein expression and enhanced punctuate dots of a green fluorescent protein tag of LC3B (Fig. 3a–d). Interestingly, LC3B protein expression dropped to basal level at 24 h suggesting that autophagy was not consistently induced by arsenic treatment. Results of TUNEL staining, PARP cleavage and FACS analysis (Figs. 1, 2) indicated that the cell death at 24 h mainly through apoptosis. To our best knowledge, this is the first study showing arsenic could induce apoptosis, as well as autophagy in HK-2 cells.

It still remains very controversial whether autophagy is protective or damaging to kidney (Kimura et al. 2010; Jiang et al. 2012). Our results showed that arsenic exposure resulted in intracellular superoxide production as early as 3 h and in a dose-dependent manner, whereas administration of antioxidant NAC efficiently suppressed ROS production (Fig. 4c, d), which was accompanied by down-regulation of apoptosis (Figs. 1, 2) and autophagy (Fig. 3). These results indicated that ROS generation was the main inducer of HK-2 apoptosis and autophagy after arsenic exposure. Based on our current findings, we speculated that autophagy as a response of HK-2 cells to the oxidative stress in the early phase after arsenic exposure; on the other hand, when oxidative stress is under control, autophagy is suppressed. This is well correlated with TMP and NAC-mediated suppression of ROS production and protection of HK-2 cells against arsenic cytotoxicity via decreased autophagy and apoptosis. Recently, a role of ROS as the inducer of autophagy has been reported (Lee et al. 2012). Meanwhile, our current findings were consistent with previous consensus that arsenic-induced cytotoxic effects were ROS-dependent (Weng et al. 2013; Srivastava et al. 2013; Kumagai and Sumi 2007). It has been demonstrated that GSH depletion was deeply involved in arsenic-induced ROS production (Yu et al. 2013;

Thompson and Franklin 2010). In agreement with these reports, decreased GSH levels were observed in HK-2 cells after arsenite exposure (Fig. 4g).

Since mitochondria are both the targets for oxidative stress and as a rich source of ROS (Burtner et al. 2009; Aung-Htut et al. 2013), we hypothesized that mitochondrial dysfunction could be involved in arsenic nephrotoxicity. We found that arsenic exposure led to altered mitochondrial morphology (data not shown). To gain further insight into the relationship between mitochondrial alterations and arsenic nephrotoxicity, we analyzed mitochondria function by Cox and SDH histochemical assay and by determination of mitochondrial membrane potential. After 6-h exposure, arsenic resulted in strong loss of mitochondrial membrane potential and decreased Cox enzyme activity (Fig. 5a–d), which indicated mitochondrial dysfunction. Consistent with the function of suppressing ROS, NAC and TMP pretreatment protects HK-2 cells against arsenic-induced mitochondrial dysfunction (Fig. 5a–d).

Another novel finding of the current study is the demonstration that arsenic exposure led to dynamic alterations of COX-2 expression in renal tubular epithelial cells. Although arsenic-induced activation of inflammatory factor has been reported in other cellular systems, the role of inflammation in arsenic nephrotoxicity is poorly understood, and there are few related data available for arsenic-treated human kidney cells (Wang et al. 2012b, 2013a, b; Xu et al. 2013). Induction of COX-2 via prostaglandins played a protective effect in acute renal failure, and selective COX-2 inhibition significantly decreased glomerular filtration rate (GFR) and renal blood flow, thereby resulting in AKI among salt-depleted patients (Hao and Breyer 2007; Swan et al. 2000). We observed a fast and well-pronounced up-regulation of COX-2 protein expression in HK-2 cells after arsenic exposure (Fig. 7c, d). Considering COX-2 function in maintaining renal function, we therefore speculate that such an increase could be self-protective. Interestingly, COX-2 upregulation is not continuous, as we observed COX-2 protein expression dropped to basal level at 24 h after arsenic exposure (Fig. 7c, d). TMP and NAC pretreatment reversed COX-2 dynamic changes, due to suppression of NF-κB activation and β-catenin protein expression, the main regulators of COX-2 gene expression (Fig. 6). To our best knowledge, this is the first study showing the dynamic changes of COX-2 involved in arsenic-induced nephrotoxicity.

We also explored the underlying signal mechanisms in modulating arsenic-induced COX-2 activation in HK-2 cells. As a protein of Wnt signaling pathway, β-catenin could act as a transcriptional factor and affect COX-2 transcription (Nunez et al. 2011). Meanwhile, β-catenin was reported to play an important role in the carcinogenic activities of arsenic (Wang et al. 2013c). We observed arsenic treatment increased β-catenin expression in the early phase (3 h), such up-regulation then gradually dropped to basal level (Fig. 6c, d). Correspondingly, arsenic-induced COX-2 expression occurred at 3 h and returned to normal at 24 h (Fig. 7c, d). Recent cancer studies revealed the multiple relationships between COX-2 and β-catenin, for example, COX-2 acted as mediator to result in enhanced activation of β-catenin signaling in nonsmall cell lung cancer cell migration (Singh and Katiyar 2013).

Additionally, NF-κB played a key role in pro-inflammatory signal response and acted as a critical target of arsenic cytotoxicity in many cell types (Op den Kamp et al. 2013; Kumagai and Sumi 2007). Previous studies from our laboratory and others showed that NF-κB served as another upstream regulator of COX-2 (Ruiz et al. 2013; Ivanov et al. 2010; Wang et al. 2013b). Our present study showed arsenic treatment substantially increased nuclear NF-κB protein expression, and such NF-κB activation was still observed at 24 h after treatment (Fig. 6a, b). Both NAC and TMP pretreatment efficiently reversed arsenic-induced nuclear NF-κB protein up-regulation suggesting that arsenic acted as an activator of NF-κB through ROS in HK-2 cell. Similar finding was also reported for many different cell systems, including endothelial cells (Wang et al. 2012b). To further confirm NF-κB as the upstream of COX-2, NF-κB inhibitor (Bay11-7082) was applied and notably blocked arsenic-induced COX-2 expression at 6 h (Fig. 8a).

As an important member of mitogen-activated protein kinase (MAPK) family, p38 MAPK was reported to act as upstream signal regulating COX-2 expression in normal human lung fibroblast after arsenic exposure(Wang et al. 2013b). Consistent with this report, we also observed increased phospho-p38 MAPK expression in HK-2 cells at 6 h after arsenic treatment. SB203580, an inhibitor of p38 MAPK, efficiently inhibited COX-2 expression induced by arsenic (Fig. 8b).

Furthermore, we detected the effect of arsenic on the critical pro-inflammatory regulator TNF-α in HK-2 cells. Arsenic treatment effectively enhanced TNF-α protein expression (Fig. 8c, d), suggesting that TNF-α also contributed to arsenic nephrotoxicity in vitro. This is in accordance with the previous report that TNF-α expression was elevated in a rat model of arsenic-induced nephrotoxicity (Prabu and Muthumani 2012). Nevertheless, attention should be paid to the report that arsenic also acts as an anti-inflammatory agent by inhibiting TNF-α in rheumatoid arthritis (Mei et al. 2010). Similar interesting but controversial observations were also observed in the effects of arsenic on NF-κB activation (Kumagai and Sumi 2007; Mei et al. 2010), perhaps reflecting a cell-specific response.

The major finding of our study was the TMP-dependent renoprotective effect against arsenic-induced cytotoxicity in HK-2 cells. Such a protection was demonstrated by enhanced cellular GSH levels and decreased levels of ROS production, autophagy and apoptosis. The mitochondrial origin of the protective effects of TMP was further evident by its mitigation of arsenic-induced mitochondrial morphology and functional changes. The biological activities of TMP showed cell selectivity. Our present findings indicated that TMP protected HK-2 cells against arsenic-induced apoptosis and on the other hand, TMP was also reported to promote arsenic trioxide toxicity and inhibit proliferation in human promyelocytic leukemia cell line HL-60 (Wu et al. 2012). Such a cell specificity of pro-apoptotic or anti-apoptotic effect of TMP was also observed in hepatocytes (Zhang et al. 2013). In addition to its anti-apoptotic activity, our data also highlighted the anti-inflammatory role of TMP in inhibiting a sequence of pro-inflammatory signal regulators, including β-catenin, NF-κB, p38 MAPK, TNF-α and COX-2. Undoubtedly, the anti-inflammation effects of TMP contributed to its protection against arsenic nephrotoxicity. The ability of TMP to block p38 MAPK activities was consistent with our previous findings in contrast-induced nephropathy in vivo (Gong et al. 2013). In China, TMP has been widely

used in the treatment of renal, cardiovascular and cerebral ischemic diseases with a high degree of safety (Wang et al. 2012a; Tang et al. 2013; Gong et al. 2013). Many clinical and experimental studies have revealed that TMP functions as a vasodilator, an anti-coagulant, a free radical scavenger and a suppressor of inflammation and apoptosis (Wang et al. 2012a; Toth et al. 2013; Kao et al. 2013).

In summary, the present study suggests that arsenic treatment at clinically relevant dose results in renal toxicity based on observation made in a human renal tubular epithelial cell model. Furthermore, such cell damage is complex, besides the known necrosis, involving apoptosis and autophagy; there is involvement of oxidative stress, pro-inflammatory signal activation and mitochondrial dysfunction as well. Finally, TMP efficiently prevents arsenic-induced nephrotoxicity in vitro by reversing these pathological processes and thus may prove beneficial in patients at high risk for arsenic-induced nephrotoxicity.

Acknowledgments

The authors would like to thank Drs. Preety Sharma, Erik Young, Bo Zhang, Gangkun Lin, Wupeng Liao, Hongning Zhou and Winsome Walker for advice and helpful discussion. This work was supported by Environmental Center Grant P30 ES009089, NIH Grant P01 CA049062 and National Natural Science Foundation of China Grant 81001509 and 81373614.

Abbreviations

AKI	Acute kidney injury
CKD	Chronic kidney disease
COX-2	Cyclooxygenase-2
DHE	Dihydroethidium
FACS	Fluorescence-activated cell sorter
GSH	Glutathione
MAPK	Mitogen-activated protein kinase
MTT	3-(4,5-Dimethylthiazol-2-yl)-2,5-diphenyltetrazolium
NAC	*N*-Acetylcysteine
NF-κB	Nuclear factor-κB
PARP	Poly ADP-ribose polymerase
PI	Propidium iodide
ROS	Reactive oxygen species
SDH	Succinate dehydrogenase
TMP	Tetramethylpyrazine
TNF-α	Tumor necrosis factor alpha
TUNEL	Terminal deoxynucleotidyl transferase-mediated dUTP-biotin nick-end labeling

References

Aung-Htut MT, Lam YT, Lim YL, Rinnerthaler M, Gelling CL, Yang H, Breitenbach M, Dawes IW. Maintenance of mitochondrial morphology by autophagy and its role in high glucose effects on chronological lifespan of *Saccharomyces cerevisiae* . Oxid Med Cell Longev. 2013; 2013:636287. [PubMed: 23936612]

Baeuerle PA, Henkel T. Function and activation of NF-kappa B in the immune system. Annu Rev Immunol. 1994; 12:141–179. [PubMed: 8011280]

Bolt AM, Byrd RM, Klimecki WT. Autophagy is the predominant process induced by arsenite in human lymphoblastoid cell lines. Toxicol Appl Pharmacol. 2010; 244(3):366–373. [PubMed: 20153345]

Burtner CR, Murakami CJ, Kennedy BK, Kaeberlein M. A molecular mechanism of chronological aging in yeast. Cell Cycle. 2009; 8(8):1256–1270. [PubMed: 19305133]

Chen JW, Chen HY, Li WF, Liou SH, Chen CJ, Wu JH, Wang SL. The association between total urinary arsenic concentration and renal dysfunction in a community-based population from central Taiwan. Chemosphere. 2011; 84(1):17–24. [PubMed: 21458841]

Eichler T, Ma Q, Kelly C, Mishra J, Parikh S, Ransom RF, Devarajan P, Smoyer WE. Single and combination toxic metal exposures induce apoptosis in cultured murine podocytes exclusively via the extrinsic caspase 8 pathway. Toxicol Sci. 2006; 90(2):392–399. [PubMed: 16421179]

Emadi A, Gore SD. Arsenic trioxide—an old drug rediscovered. Blood Rev. 2010; 24(4–5):191–199. [PubMed: 20471733]

Fan SF, Chao PL, Lin AM. Arsenite induces oxidative injury in rat brain: synergistic effect of iron. Ann NY Acad Sci. 2010; 1199:27–35. [PubMed: 20633106]

Gong X, Celsi G, Carlsson K, Norgren S, Chen M. N-Acetylcysteine amide protects renal proximal tubular epithelial cells against iohexol-induced apoptosis by blocking p38 MAPK and iNOS signaling. Am J Nephrol. 2010; 31(2):178–188. [PubMed: 20016144]

Gong X, Wang Q, Tang X, Wang Y, Fu D, Lu H, Wang G, Norgren S. Tetramethylpyrazine prevents contrast-induced nephropathy by inhibiting p38 MAPK and FoxO1 signaling pathways. Am J Nephrol. 2013; 37(3):199–207. [PubMed: 23446291]

Graef M, Nunnari J. Mitochondria regulate autophagy by conserved signalling pathways. EMBO J. 2011; 30(11):2101–2114. [PubMed: 21468027]

Hao CM, Breyer MD. Physiologic and pathophysiologic roles of lipid mediators in the kidney. Kidney Int. 2007; 71(11):1105–1115. [PubMed: 17361113]

Ivanov VN, Hei TK. Arsenite sensitizes human melanomas to apoptosis via tumor necrosis factor alpha-mediated pathway. J Biol Chem. 2004; 279(21):22747–22758. [PubMed: 15028728]

Ivanov VN, Hei TK. Combined treatment with EGFR inhibitors and arsenite upregulated apoptosis in human EGFR-positive melanomas: a role of suppression of the PI3K-AKT pathway. Oncogene. 2005; 24(4):616–626. [PubMed: 15580309]

Ivanov VN, Hei TK. Induction of apoptotic death and retardation of neuronal differentiation of human neural stem cells by sodium arsenite treatment. Exp Cell Res. 2013; 319(6):875–887. [PubMed: 23219847]

Ivanov VN, Zhou H, Ghandhi SA, Karasic TB, Yaghoubian B, Amundson SA, Hei TK. Radiation-induced bystander signaling pathways in human fibroblasts: a role for interleukin-33 in the signal transmission. Cell Signal. 2010; 22(7):1076–1087. [PubMed: 20206688]

Ivanov VN, Wen G, Hei TK. Sodium arsenite exposure inhibits AKT and Stat3 activation, suppresses self-renewal and induces apoptotic death of embryonic stem cells. Apoptosis. 2013; 18(2):188–200. [PubMed: 23143138]

Jiang M, Wei Q, Dong G, Komatsu M, Su Y, Dong Z. Autophagy in proximal tubules protects against acute kidney injury. Kidney Int. 2012; 82(12):1271–1283. [PubMed: 22854643]

Juan SH, Chen CH, Hsu YH, Hou CC, Chen TH, Lin H, Chu YL, Sue YM. Tetramethylpyrazine protects rat renal tubular cell apoptosis induced by gentamicin. Nephrol Dial Transplant. 2007; 22(3):732–739. [PubMed: 17132701]

Kao TK, Chang CY, Ou YC, Chen WY, Kuan YH, Pan HC, Liao SL, Li GZ, Chen CJ. Tetramethylpyrazine reduces cellular inflammatory response following permanent focal cerebral ischemia in rats. Exp Neurol. 2013; 247:188–201. [PubMed: 23644042]

Kimura A, Ishida Y, Wada T, Hisaoka T, Morikawa Y, Sugaya T, Mukaida N, Kondo T. The absence of interleukin-6 enhanced arsenite-induced renal injury by promoting autophagy of tubular epithelial cells with aberrant extracellular signal-regulated kinase activation. Am J Pathol. 2010; 176(1):40–50. [PubMed: 20008137]

Kumagai Y, Sumi D. Arsenic: signal transduction, transcription factor, and biotransformation involved in cellular response and toxicity. Annu Rev Pharmacol Toxicol. 2007; 47:243–262. [PubMed: 17002598]

Lau A, Zheng Y, Tao S, Wang H, Whitman SA, White E, Zhang DD. Arsenic inhibits autophagic flux, activating the Nrf2-Keap1 pathway in a p62-dependent manner. Mol Cell Biol. 2013; 33(12): 2436–2446. [PubMed: 23589329]

Lee J, Giordano S, Zhang J. Autophagy, mitochondria and oxidative stress: cross-talk and redox signalling. Biochem J. 2012; 441(2):523–540. [PubMed: 22187934]

Martin-Pardillos A, Sosa C, Sorribas V. Arsenic increases Pimediated vascular calcification and induces premature senescence in vascular smooth muscle cells. Toxicol Sci. 2013; 131(2):641–653. [PubMed: 23104429]

Mei Y, Zheng Y, Wang H, Gao J, Liu D, Zhao Y, Zhang Z. Arsenic trioxide induces apoptosis of fibroblast-like synovio-cytes and represents antiarthritis effect in experimental model of rheumatoid arthritis. J Rheumatol. 2010; 38(1):36–43. [PubMed: 20889596]

Michael HA. Geochemistry. An arsenic forecast for China. Science. 2013; 341(6148):852–853. [PubMed: 23970688]

Nunez F, Bravo S, Cruzat F, Montecino M, De Ferrari GV. Wnt/beta-catenin signaling enhances cyclooxygenase-2 (COX2) transcriptional activity in gastric cancer cells. PLoS ONE. 2011; 6(4):e18562. [PubMed: 21494638]

Op den Kamp CM, Langen RC, Snepvangers FJ, de Theije CC, Schellekens JM, Laugs F, Dingemans AM, Schols AM. Nuclear transcription factor kappa B activation and protein turnover adaptations in skeletal muscle of patients with progressive stages of lung cancer cachexia. Am J Clin Nutr. 2013; 98(3):738–748. [PubMed: 23902785]

Partridge MA, Huang SX, Hernandez-Rosa E, Davidson MM, Hei TK. Arsenic induced mitochondrial DNA damage and altered mitochondrial oxidative function: implications for genotoxic mechanisms in mammalian cells. Cancer Res. 2007; 67(11):5239–5247. [PubMed: 17545603]

Peraza MA, Carter DE, Gandolfi AJ. Toxicity and metabolism of subcytotoxic inorganic arsenic in human renal proximal tubule epithelial cells (HK-2). Cell Biol Toxicol. 2003; 19(4):253–264. [PubMed: 14686617]

Prabu SM, Muthumani M. Silibinin ameliorates arsenic induced nephrotoxicity by abrogation of oxidative stress, inflammation and apoptosis in rats. Mol Biol Rep. 2012; 39(12):11201–11216. [PubMed: 23070905]

Rodriguez-Lado L, Sun G, Berg M, Zhang Q, Xue H, Zheng Q, Johnson CA. Groundwater arsenic contamination throughout China. Science. 2013; 341(6148):866–868. [PubMed: 23970694]

Ruiz S, Pergola PE, Zager RA, Vaziri ND. Targeting the transcription factor Nrf2 to ameliorate oxidative stress and inflammation in chronic kidney disease. Kidney Int. 2013; 83(6):1029–1041. [PubMed: 23325084]

Salviati L, Hernandez-Rosa E, Walker WF, Sacconi S, DiMauro S, Schon EA, Davidson MM. Copper supplementation restores cytochrome c oxidase activity in cultured cells from patients with SCO2 mutations. Biochem J. 2002; 363(Pt 2):321–327. [PubMed: 11931660]

Schreiber E, Matthias P, Muller MM, Schaffner W. Rapid detection of octamer binding proteins with ‘mini-extracts’, prepared from a small number of cells. Nucleic Acids Res. 1989; 17(15):6419. [PubMed: 2771659]

Shen ZX, Chen GQ, Ni JH, Li XS, Xiong SM, Qiu QY, Zhu J, Tang W, Sun GL, Yang KQ, Chen Y, Zhou L, Fang ZW, Wang YT, Ma J, Zhang P, Zhang TD, Chen SJ, Chen Z, Wang ZY. Use of arsenic trioxide (As2O3) in the treatment of acute promyelocytic leukemia (APL): II. Clinical

efficacy and pharmacokinetics in relapsed patients. Blood. 1997; 89(9):3354–3360. [PubMed: 9129042]

Singh T, Katiyar SK. Honokiol inhibits non-small cell lung cancer cell migration by targeting PGE(2)-mediated activation of beta-catenin signaling. PLoS ONE. 2013; 8(4):e60749. [PubMed: 23580348]

Soignet SL, Maslak P, Wang ZG, Jhanwar S, Calleja E, Dardashti LJ, Corso D, DeBlasio A, Gabrilove J, Scheinberg DA, Pandolfi PP, Warrell RP Jr. Complete remission after treatment of acute promyelocytic leukemia with arsenic trioxide. N Engl J Med. 1998; 339(19):1341–1348. [PubMed: 9801394]

Srivastava RK, Li C, Chaudhary SC, Ballestas ME, Elmets CA, Robbins DJ, Matalon S, Deshane JS, Afaq F, Bickers DR, Athar M. Unfolded protein response (UPR) signaling regulates arsenic trioxide-mediated macrophage innate immune function disruption. Toxicol Appl Pharmacol. 2013

Swan SK, Rudy DW, Lasseter KC, Ryan CF, Buechel KL, Lambrecht LJ, Pinto MB, Dilzer SC, Obrda O, Sundblad KJ, Gumbs CP, Ebel DL, Quan H, Larson PJ, Schwartz JI, Musliner TA, Gertz BJ, Brater DC, Yao SL. Effect of cyclooxygenase-2 inhibition on renal function in elderly persons receiving a low-salt diet. A randomized, controlled trial. Ann Intern Med. 2000; 133(1):1–9. [PubMed: 10877734]

Tang Z, Wang Q, Xu H, Zhang W. Microdialysis sampling for investigations of tetramethylpyrazine following transdermal and intraperitoneal administration. Eur J Pharm Sci. 2013

Thompson JA, Franklin CC. Enhanced glutathione biosynthetic capacity promotes resistance to As3+induced apoptosis. Toxicol Lett. 2010; 193(1):33–40. [PubMed: 20006689]

Toth S Jr, Pekarova T, Varga J, Toth S, Tomeckova V, Gal P, Vesela J, Guzy J. Intravenous administration of tetramethylpyrazine reduces intestinal ischemia-reperfusion injury in rats. Am J Chin Med. 2013; 41(4):817–829. [PubMed: 23895154]

Wang B, Ni Q, Wang X, Lin L. Meta-analysis of the clinical effect of ligustrazine on diabetic nephropathy. Am J Chin Med. 2012a; 40(1):25–37. [PubMed: 22298446]

Wang L, Kou MC, Weng CY, Hu LW, Wang YJ, Wu MJ. Arsenic modulates heme oxygenase-1, interleukin-6, and vascular endothelial growth factor expression in endothelial cells: roles of ROS, NF-kappaB, and MAPK pathways. Arch Toxicol. 2012b; 86(6):879–896. [PubMed: 22488045]

Wang H, Xi S, Xu Y, Wang F, Zheng Y, Li B, Li X, Zheng Q, Sun G. Sodium arsenite induces cyclooxygenase-2 expression in human uroepithelial cells through MAPK pathway activation and reactive oxygen species induction. Toxicol In Vitro. 2013a; 27(3):1043–1048. [PubMed: 23376440]

Wang Q, Wu L, Wang J. Reciprocal regulation of cyclooxygenase 2 and heme oxygenase 1 upon arsenic trioxide exposure in normal human lung fibroblast. J Biochem Mol Toxicol. 2013b; 27(6): 323–329. [PubMed: 23649692]

Wang X, Mandal AK, Saito H, Pulliam JF, Lee EY, Ke ZJ, Lu J, Ding S, Li L, Shelton BJ, Tucker T, Evers BM, Zhang Z, Shi X. Arsenic and chromium in drinking water promote tumo-rigenesis in a mouse colitis-associated colorectal cancer model and the potential mechanism is ROS-mediated Wnt/beta-catenin signaling pathway. Toxicol Appl Pharmacol. 2013c; 262(1):11–21. [PubMed: 22552367]

Weng CY, Chiou SY, Wang L, Kou MC, Wang YJ, Wu MJ. Arsenic trioxide induces unfolded protein response in vascular endothelial cells. Arch Toxicol. 2013

Wu J, Song R, Song W, Li Y, Zhang Q, Chen Y, Fu Y, Fang W, Wang J, Zhong Z, Ling H, Zhang L, Zhang F. Chlorpromazine protects against apoptosis induced by exogenous stimuli in the developing rat brain. PLoS ONE. 2011; 6(7):e21966. [PubMed: 21779358]

Wu Y, Xu Y, Shen Y, Wang C, Guo G, Hu T. Tetramethylpyrazine potentiates arsenic trioxide activity against HL-60 cell lines. Braz J Med Biol Res. 2012; 45(3):187–196. [PubMed: 22331136]

Xu Y, Zhao Y, Xu W, Luo F, Wang B, Li Y, Pang Y, Liu Q. Involvement of HIF-2alpha-mediated inflammation in arsenite-induced transformation of human bronchial epithelial cells. Toxicol Appl Pharmacol. 2013

Yamamoto Y, Sasaki M, Oshimi K, Sugimoto K. Arsenic trioxide in a hemodialytic patient with acute promyelocytic leukemia. Acta Haematol. 2009; 122(1):52–53. [PubMed: 19816009]

Yen YP, Tsai KS, Chen YW, Huang CF, Yang RS, Liu SH. Arsenic induces apoptosis in myoblasts through a reactive oxygen species-induced endoplasmic reticulum stress and mitochondrial dysfunction pathway. Arch Toxicol. 2012; 86(6):923–933. [PubMed: 22622864]

Yu M, Xue J, Li Y, Zhang W, Ma D, Liu L, Zhang Z. Resveratrol protects against arsenic trioxide-induced nephrotoxicity by facilitating arsenic metabolism and decreasing oxidative stress. Arch Toxicol. 2013; 87(6):1025–1035. [PubMed: 23471352]

Zhai L, Zhang P, Sun RY, Liu XY, Liu WG, Guo XL. Cytoprotective effects of CSTMP, a novel stilbene derivative, against H2O2-induced oxidative stress in human endothelial cells. Pharmacol Rep. 2012; 63(6):1469–1480. [PubMed: 22358095]

Zhang F, Kong DS, Zhang ZL, Lei N, Zhu XJ, Zhang XP, Chen L, Lu Y, Zheng SZ. Tetramethylpyrazine induces G0/G1 cell cycle arrest and stimulates mitochondrial-mediated and caspase-dependent apoptosis through modulating ERK/p53 signaling in hepatic stellate cells in vitro. Apoptosis. 2013; 18(2):135–149. [PubMed: 23247439]

Zhao XY, Li GY, Liu Y, Chai LM, Chen JX, Zhang Y, Du ZM, Lu YJ, Yang BF. Resveratrol protects against arsenic trioxide-induced cardiotoxicity in vitro and in vivo. Br J Pharmacol. 2008; 154(1): 105–113. [PubMed: 18332854]

Zheng LY, Umans JG, Tellez-Plaza M, Yeh F, Francesconi KA, Goessler W, Silbergeld EK, Guallar E, Howard BV, Weaver VM, Navas-Acien A. Urine arsenic and prevalent albuminuria: evidence from a population-based study. Am J Kidney Dis. 2013; 61(3):385–394. [PubMed: 23142528]

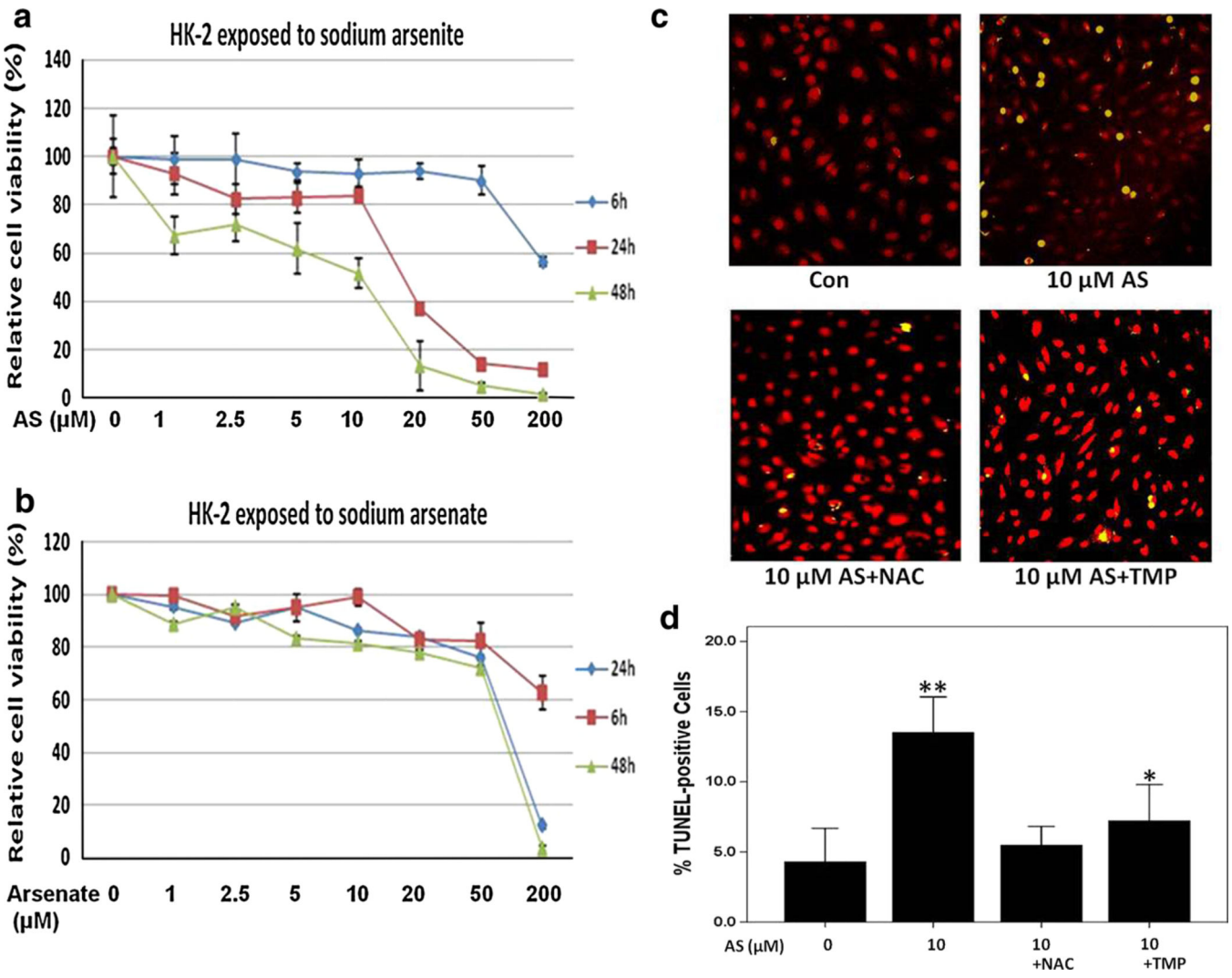

Fig. 1.

TMP prevented arsenic-induced cytotoxicity and apoptosis in HK-2 cells. **a, b** HK-2 cells were incubated with sodium arsenite or sodium arsenate at different doses for 6, 24 or 48 h. Cell viability was measured by MTT assay. **c** Apoptosis was determined by TUNEL and PI staining. HK-2 cells were exposed to sodium arsenite (0 or 10 μM) 24 h alone or in a combination with 10 mM NAC or 100 μM TMP. Merged images were captured by confocal fluorescent microscope at 200× magnification. **d** Average percentages of TUNEL-positive cells were assessed in each group. Values are mean ± SD ($n = 3$), *$p < 0.05$ versus control (Con), **$p < 0.01$ versus Con

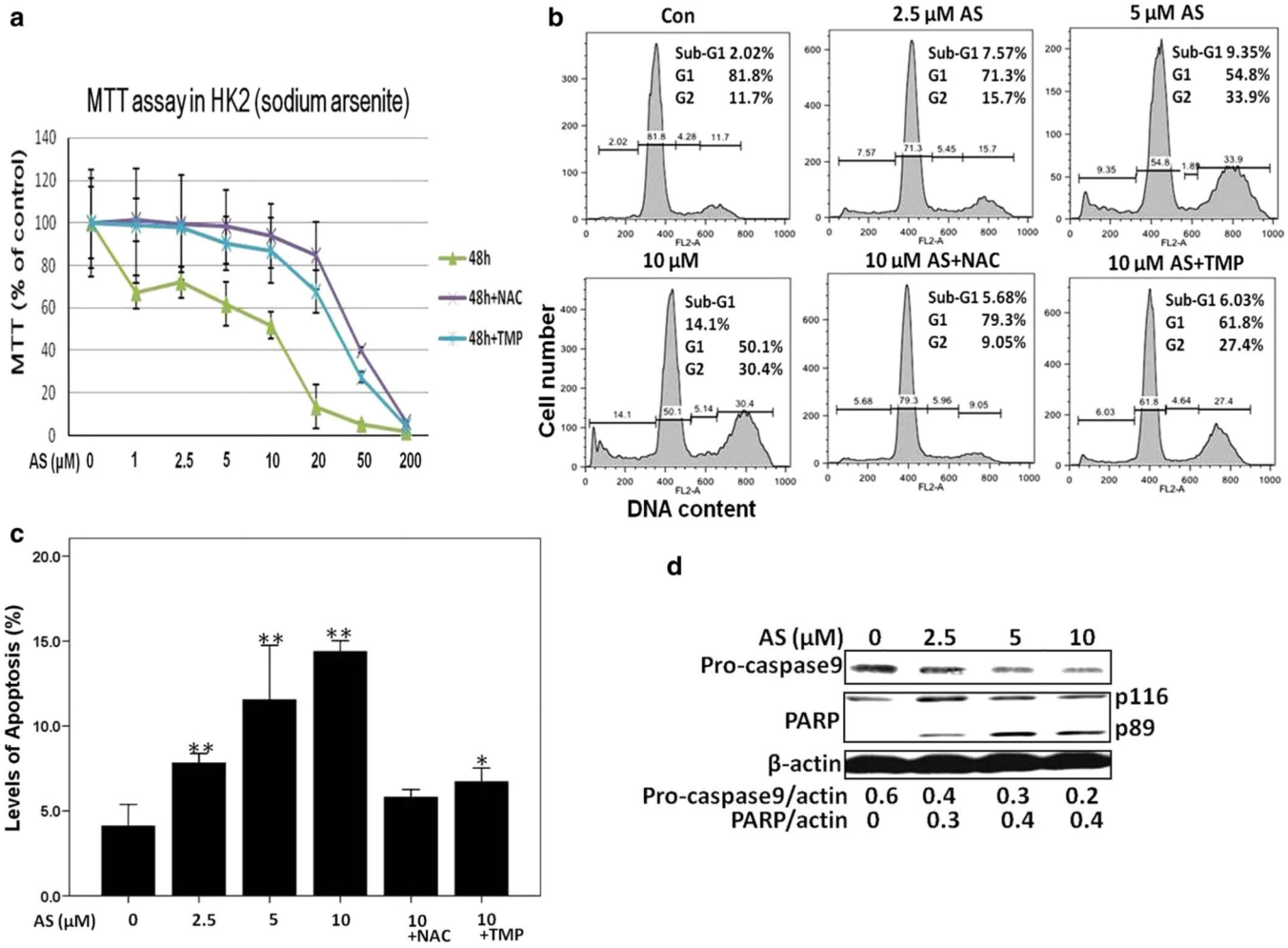

Fig. 2.

TMP and NAC inhibited arsenic-induced cytotoxicity and apoptosis in HK-2 cells determined with MTT assay, FACS by PI staining and Western blotting. **a** 100 μM TMP and 10 mM NAC pretreatment significantly increased cell viability after 48 h exposure to 10 μM sodium arsenite. **b** Apoptosis and cell cycle analysis 24 h after arsenic treatment with or without NAC (10 mM) or TMP (100 μM) pretreatment in HK-2 cells. **c** Apoptotic rate was calculated by evaluating the percentage of events accumulated in the sub-G1 position. **d** Procaspase-9 protein expression and PARP cleavage were examined by Western blotting using β-actin as a loading control. Values are mean ± SD ($n = 3$), *$p < 0.05$ versus Con, **$p < 0.01$ versus Con

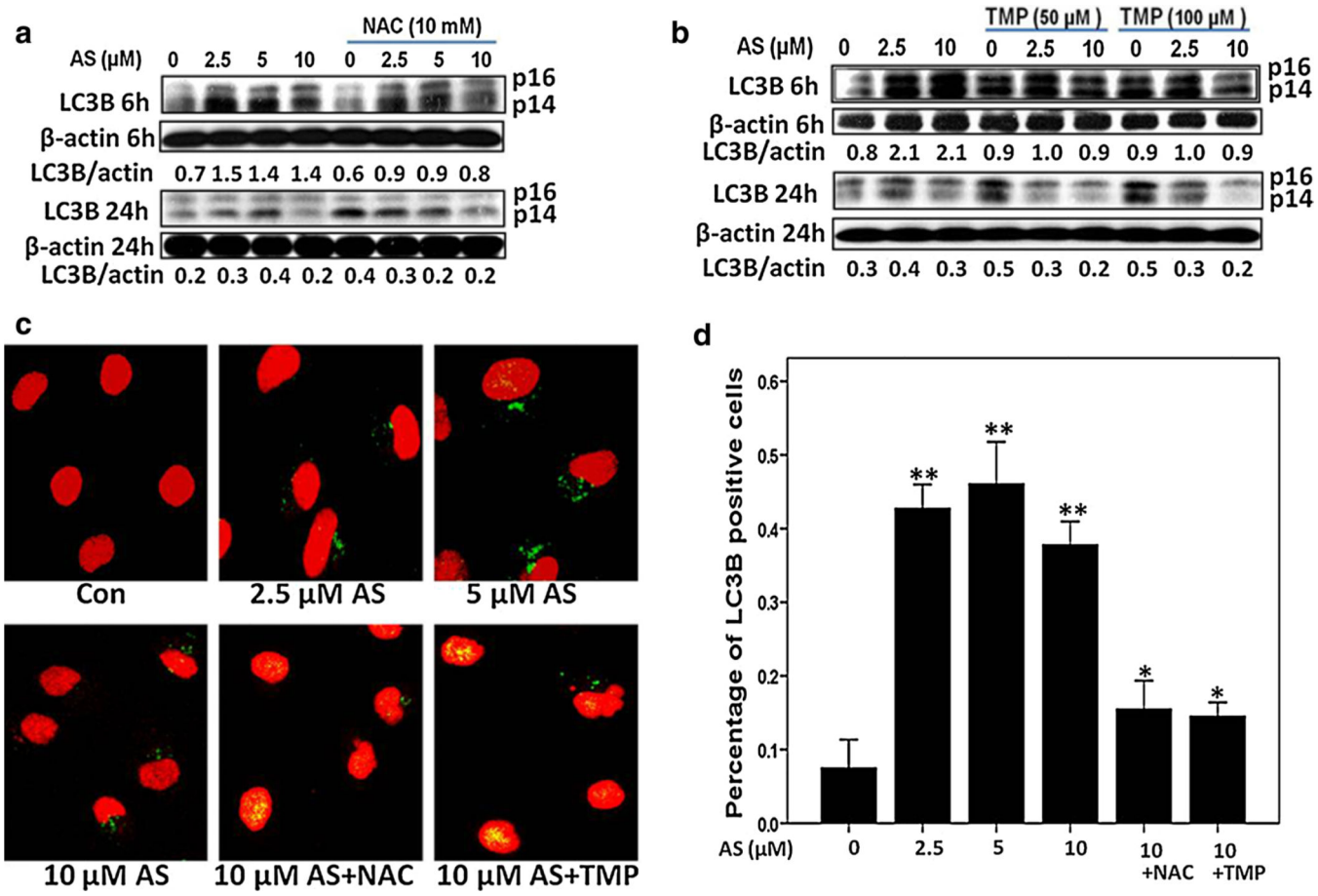

Fig. 3.

Arsenic-induced autophagy in HK-2 cells. **a, b** Arsenic treatment increased LC3B protein expression at 6 h, which dropped at 24 h. Both TMP (100 μM) and NAC (10 mM) inhibited arsenic-induced LC3B protein expression. β-Actin was used as loading control. **c, d** Induction of autophagy after 6-h arsenic exposure was visualized by LC3B staining (*green*), which was suppressed by 100 μM TMP or 10 mM NAC pretreatment. Values are mean ± SD ($n = 3$), *$p < 0.05$ versus Con, **$p < 0.01$ versus Con (color figure online)

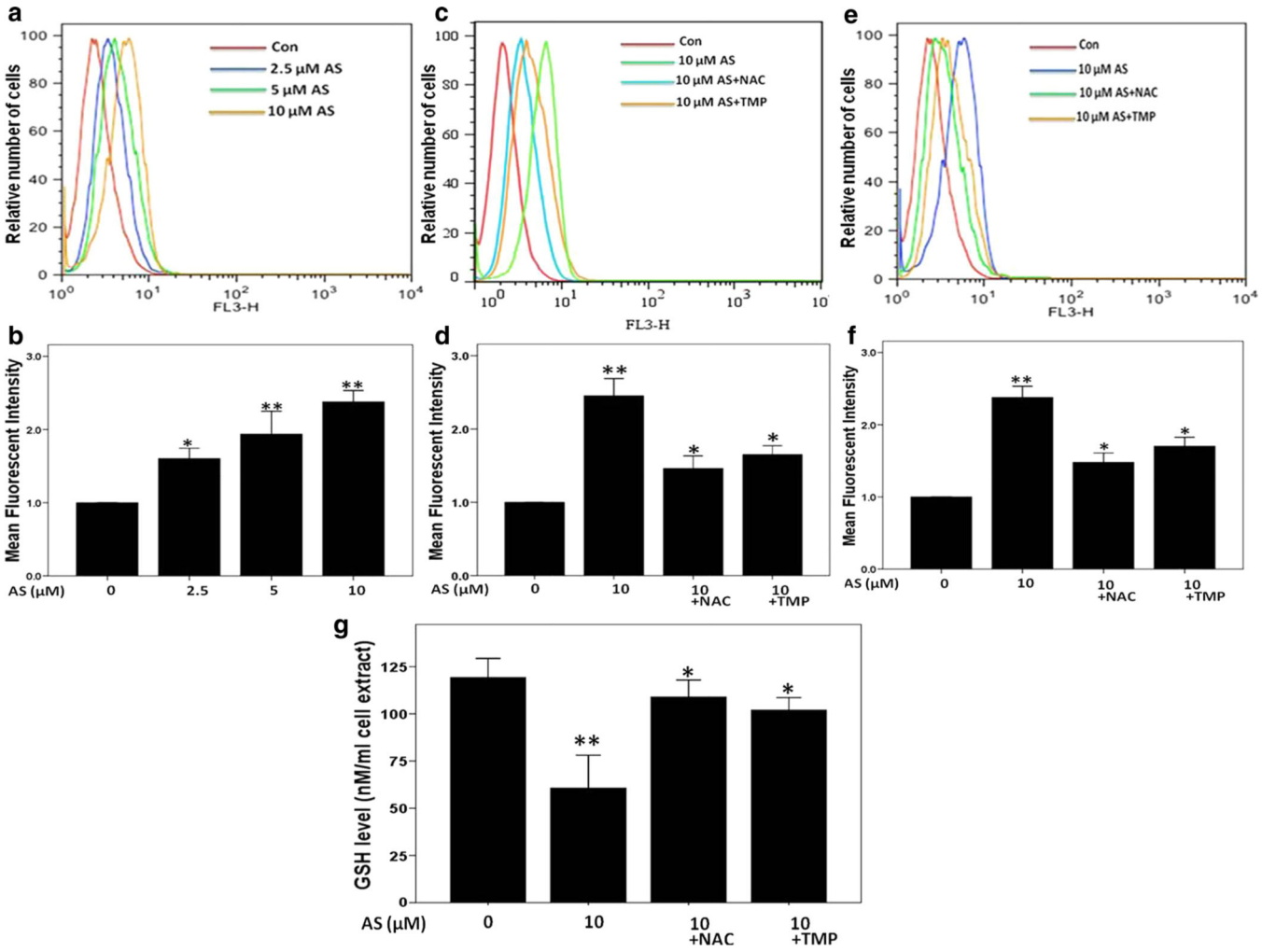

Fig. 4.

TMP and NAC suppressed arsenic-induced intracellular ROS production in HK-2 cells determined by dihydroethidium (DHE) staining and FACS analysis. **a, b** Induction of intracellular ROS generation in a dose-dependent manner. TMP (100 μM) and NAC (10 mM) inhibited arsenic-induced ROS generation at 3 (**c, d**) and 24 h (**e, f**). **g** Intracellular GSH levels were measured after 24-h sodium arsenite exposure. Values are mean ± SD (n = 3), *p < 0.05 versus Con, **p < 0.01 versus Con

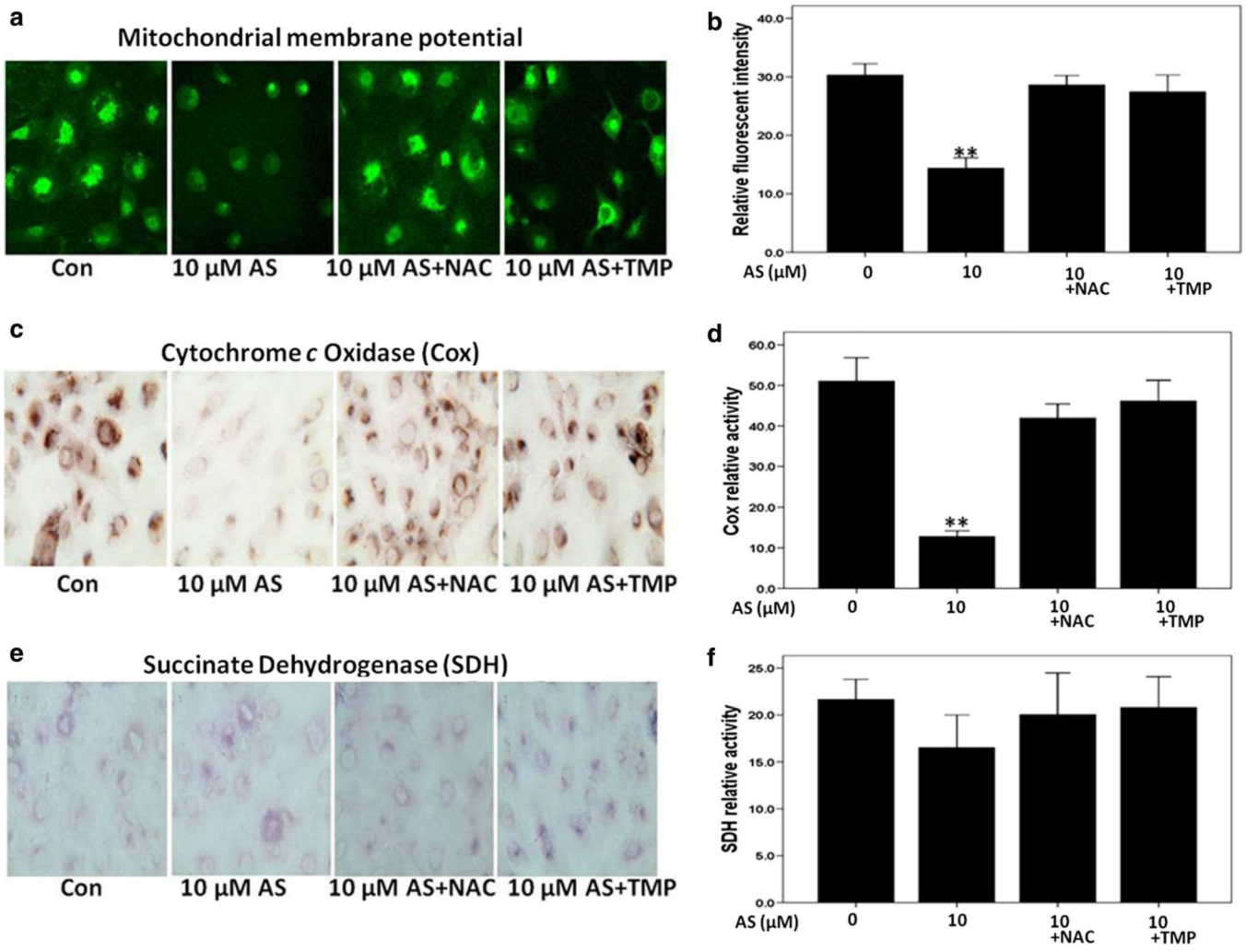

Fig. 5.

Pretreatment with 100 μM TMP or 10 mM NAC efficiently reversed arsenic-induced mitochondrial dysfunction in HK-2 cells. **a, b** Arsenic decreased mitochondrial membrane potential in HK-2 cells, while TMP and NAC prevented such a down-regulation. **c, d** Arsenic-induced mitochondrial dysfunction was verified by a decreased cytochrome *c* oxidase (Cox) histochemical staining. **e, f** Succinate dehydrogenase histochemical staining. Values are mean ± SD ($n = 3$), *$p < 0.05$ versus Con, **$p < 0.01$ versus Con

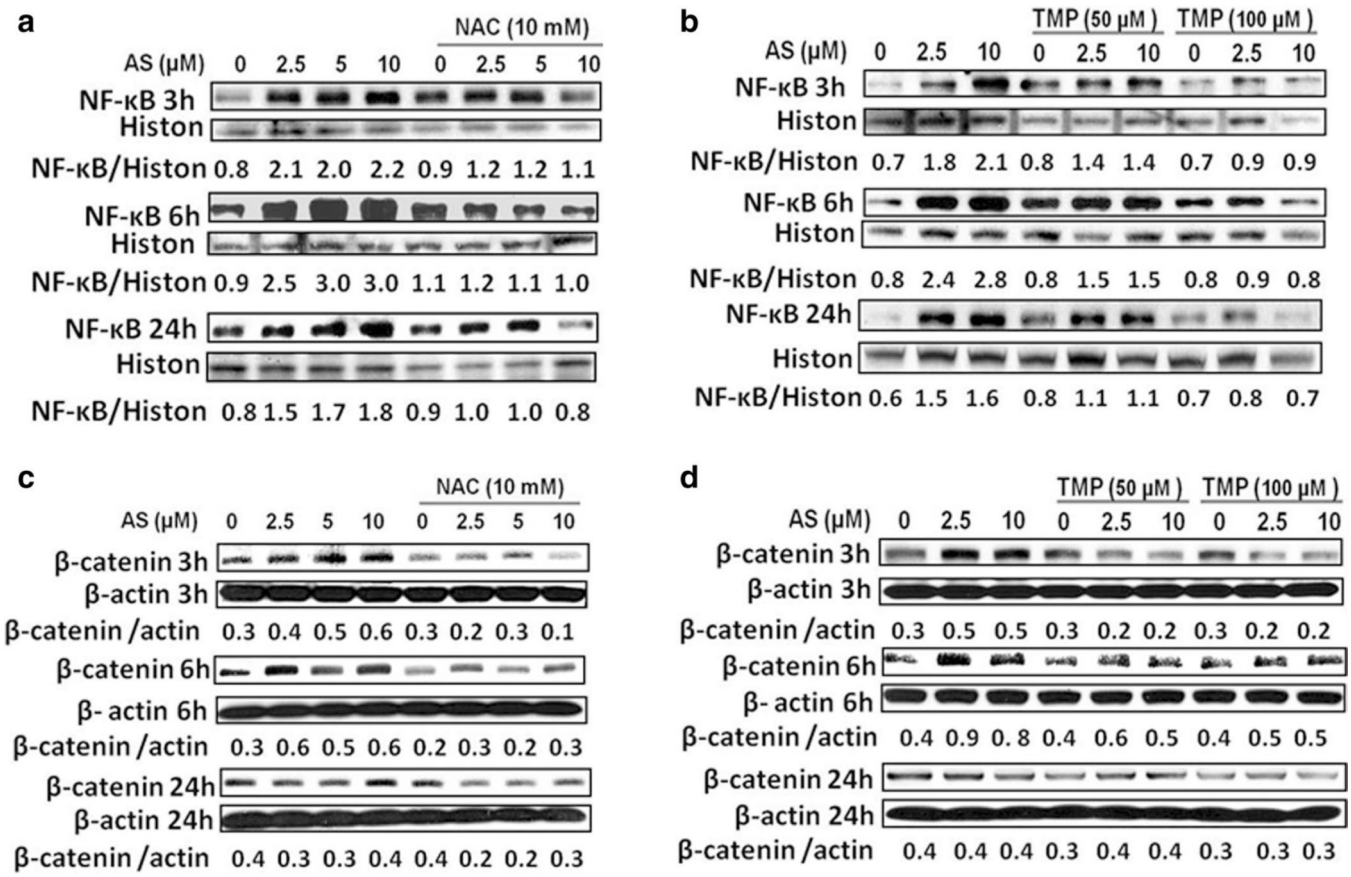

Fig. 6.

TMP and NAC inhibited arsenic-induced pro-inflammatory signals: NF-κB activation and β-catenin up-regulation in HK-2 cells. **a, b** Arsenic-induced NF-κB activation was determined by increased levels of nuclear phospho-Ser536 NF-κB p65, which was inhibited by NAC or TMP pretreatment. **c, d** Arsenic-induced β-catenin upregulation was suppressed by NAC and TMP pretreatment. Histone H3 (Histon) and β-actin were used as loading controls for nuclear and total proteins, respectively

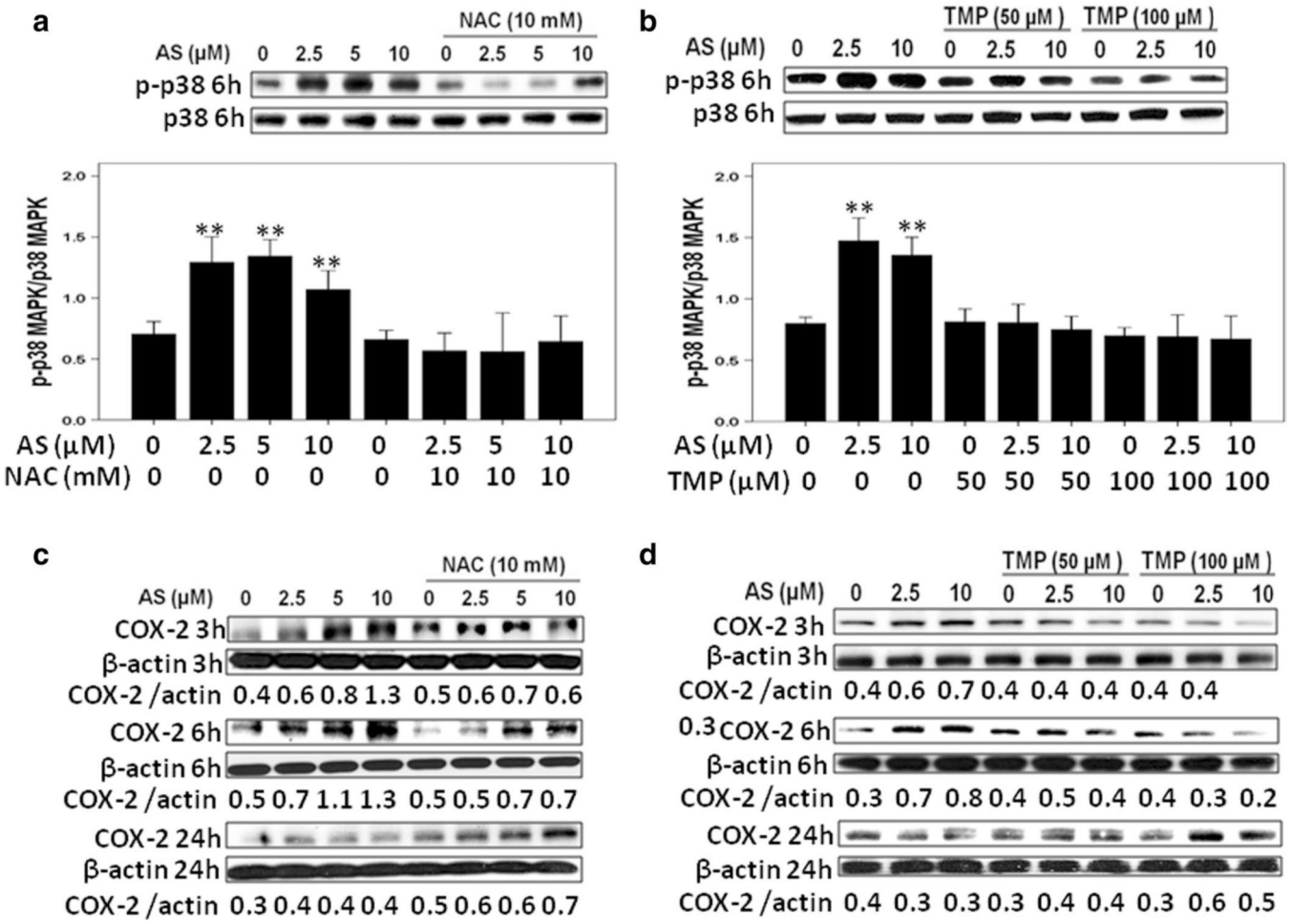

Fig. 7.

TMP and NAC inhibited arsenic-induced pro-inflammatory signals: p38 MAPK activation and COX-2 up-regulation in HK-2 cells. **a, b** Arsenic-induced p38 MAPK activation was verified by increased levels of phospho-Thr180/Tyr182 p38 MAPK (p-p38) expression, which was inhibited by NAC or TMP pretreatment. **c, d** Arsenic up-regulated COX-2 protein expression, while NAC and TMP suppressed COX-2 protein up-regulation. β-Actin was used as loading control. Values are mean ± SD ($n = 3$), $^{**}p < 0.01$ versus Con

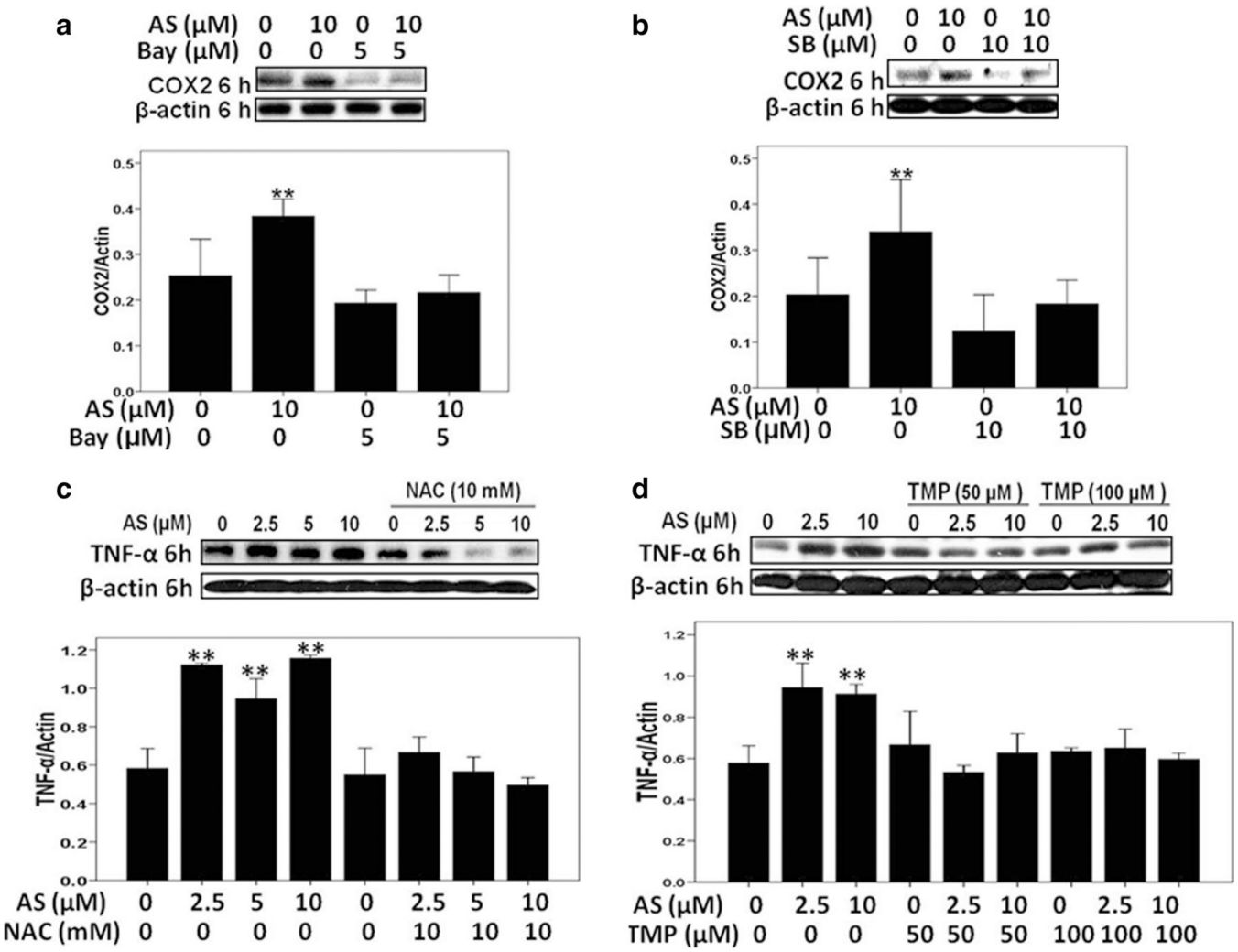

Fig. 8.

a, b Arsenic-induced COX-2 up-regulation was NF-κB- and p38 MAPK-dependent. Effects of NF-κB inhibitor (Bay11-7082) and p38 inhibitor SB203580. **c, d** Arsenic-induced TNF-α up-regulation was suppressed by TMP and NAC pretreatment. β-Actin was used as loading control. Values are mean ± SD (n = 3), $^{**}p < 0.01$ versus Con